Stationary population inversion of hydrogen in an arc-heated magnetically trapped expanding hydrogen-helium plasma jet

Hiroshi Akatsuka and Masaaki Suzuki
Research Laboratory for Nuclear Reactors, Tokyo Institute of Technology, 2-12-1 O-okayama, Meguroku, Tokyo 152, Japan
(Received 26 August 1993)

A stationary recombining hydrogen-helium mixed plasma is generated in the arc-heated magnetically trapped expanding plasma jet that was developed in the authors' laboratory. The plasma can be generated very stably and a spectroscopic analysis is accomplished with sufficient accuracy. Population densities of atomic hydrogen whose principal quantum number is 3–12 are observed spectroscopically. When the plasma comes downstream, the electron temperature becomes low and population inversion is obtained between the level pairs 3-4, 3-5, and 4-5 in hydrogen atoms. The experimental results are explained very well by a calculation based on the collisional radiative model in which the hydrogen plasma is optically thin. The potential for cw lasing by H I is discussed in terms of atomic processes based on the experimental and numerical results.

PACS number(s): 52.20.−j, 34.90.+q, 42.55.−f, 52.25.Rv

I. INTRODUCTION

About three decades have passed since the first proposal was made that the recombining plasma would be applied to the active laser medium [1]. Recently many authors have examined the potential for lasing by pulsed-laser-produced recombining plasmas to create short-wavelength lasers [2–4]. A pulsed discharge and a rapid expansion of the plasma also made pulsed recombination lasing [5,6]. As for the cw lasing, stationary population inversions have been obtained by many authors [7–13]. Up to the present time, however, the continuous plasma discharge and the following expansion have not enabled us to oscillate cw lasers due to the experimental limitations. Hara *et al.*, developed a quasi-cw laser by a recombining hydrogen plasma, whose pulse length was about several hundred microseconds [6]. But in their experiment, the rapid cooling of electrons was accomplished mainly by an adiabatic expansion and the duration of the laser oscillation was limited by the capacity of the electric power supplier.

Otsuka, Ikee, and Ishii reported that contact with a neutral gas was effective for the rapid cooling of the electrons in a helium plasma to make inverted populations [14]. Both elastic and inelastic collisions with the cold gas were used to cool electrons [15]. However, the plasma in their apparatus named TPD-I was spouted rather slowly through a large nozzle into a lower pressure space where the conductance of the gas was small. The velocity of the plasma jet was $\sim 10^3$ m/s and the diameter of the nozzle was 8–15 mm [16]. In order to cool the plasma rapidly, the plasma should be moved as fast as possible. Neutral species in the plasma especially should be expanded rapidly because the temperature of the contact gases should be low. The rapid expansion also helps decrease the optical thickness. In general, the optical thickness is an obstacle to making population inversions. The expansion was insufficient in their method and it leaves some room for improvement. Moreover, it was shown numerically that the electron density should not be too low to create the large population inversion although the electron temperature should be as low as possible [17,18]. Therefore it is considered that the magnetic confinement of the recombining plasma is efficient for the lasing.

We developed an arc-heated magnetically trapped expanding plasma jet generator, where an arc-heated thermal plasma was continuously spouted from a small nozzle of ~ 1 mm diameter into a large rarefied gas wind tunnel with a parallel magnetic field, for the purpose of applications of a thermal and a recombining plasma [19]. It was found that it produced the recombining helium plasma like an afterglow with low electron temperature continuously. Spectroscopic observations showed that the inverted populations between several level pairs in He I, such as $4\,^1S$-$3\,^1P$ and $4\,^3P$-$3\,^3D$, were created stationarily [20]. There were two important parameters for making inverted populations in the plasma generator. One was the magnetic field and the other was the pressure in the plasma expanding region. When the plasma was generated, the stronger magnetic field made the population inversion much larger. It showed that the magnetic confinement of the cold plasma was efficient to keep the electron density optimum and to create larger inversions. On the other hand, the population inversion became large when the pressure in the expanding region was about 3–20 Pa. When the pressure was made much lower, the observed inversion became smaller. Therefore it was concluded that the cooling of electrons was accomplished mainly by the collisions with the residual gases in the wind tunnel, not by the adiabatic expansion. However, we are sorry to say that the observed inversion was still insufficient for us to oscillate a cw recombining laser, because the electron density was small and the existence of the residual helium atoms in the wind tunnel made the plasma optically thick for the transitions to the ground state.

Although we examined only the helium plasma in the previous paper [19,20], the plasma generator can produce

recombining plasmas of various species, provided that the ordinary arc discharge is accomplished stably and continuously, which will result in another interesting potential for the cw lasing. We consider that the first and best alternative is the hydrogen plasma. The oscillator strengths of hydrogen atoms were calculated accurately [21]. The numerical analysis of the population density of each level is also available in the hydrogen plasma [22]. Another experimental merit of the hydrogen plasma is that the hydrogen atoms in the residual gas will make diatomic molecules. It means that the optical thickness of the hydrogen plasma, an obstacle to make the inversion, is expected to be smaller than that of the helium.

The temperature of the plasma in the arc region in our apparatus was about 1–2 eV [19], and lower than that in TPD-I [14]. Therefore the hydrogen plasma was generated not by the contact of hydrogen gas with the helium plasma jet in the downstream but by mixing the hydrogen gas into the discharging helium gas. Namely, the helium gas took a role as a buffer gas in the discharging region. The pure hydrogen plasma was difficult for us to generate stably. The stationary population inversion of H I had been observed as a minor impurity in the discharge of some kinds of rare gas [7,9]. However, the magnetic field was seldom applied there. In addition, the expansion ratio of the plasma and the pumping speed in the plasma expanding chamber are much larger in our apparatus. The plasma in our apparatus is generated continuously and very stably; therefore it is observed with a sufficient accuracy. A continuous recombining plasma such as an afterglow plasma can be generated and the spectroscopic characteristics are examined in detail, which was difficult by a conventional afterglow plasma operated like a pulse. In the present experiments, the hydrogen-helium mixed plasma is cooled rapidly into a state of nonequilibrium by collisions with residual hydrogen and helium. Therefore it has an aspect of a fundamental study on the atomic processes in a boundary plasma such as a divertor plasma of a nuclear fusion reactor.

In this paper, we describe the results of the spectroscopic observations of the hydrogen-helium mixed plasma generated by the arc-heated magnetically trapped expanding plasma jet generator. The population densities of H I in the plasma are examined and the variations of them are also investigated when the plasma comes downstream. Then the potential for cw lasing by the plasma is discussed. The experimental results are compared with the calculation based on the collisional radiative model [22] and the characteristics of the plasma are discussed in terms of atomic processes.

II. EXPERIMENTAL SETUP

The plasma generator was the same as described in Ref. [19]. A brief account is given below. The plasma generator was placed in a large rarefied gas wind tunnel, 1.2 m in diameter and 2 m in length. It was evacuated with a 12-in. mechanical booster and a 4-in. rotary pump, whose pumping speed was about 10 m^3/s at about 1 Pa with an ultimate pressure of 0.4 Pa. The plasma was expanded in the wind tunnel continuously. The discharge was very stable for the spectroscopic observations. The design of the plasma generator was the same as that of an ordinary thermal plasma torch. The anode was made of copper and has a nozzle of 0.8 mm diameter. The cathode was a 3-mm rod of 98% tungsten and 2% thorium. The electrodes were cooled by water and the electrode gap length was controlled by a motor connected to the cathode. The plasma generated by the arc discharge under relatively high pressure (1.0×10^4–1.0×10^5 Pa) was spouted through the nozzle into the wind tunnel. This discharge was generated with a magnetic field so that the nozzle might be choked with the viscous arc plasma. The viscosity of the arc plasma maintained the pressure difference between the arc discharging region and the plasma expanding region. Six coreless coils of 80 mm i.d. and of 60 mm thickness were placed with a 10-mm gap coaxially with the plasma torch axis and the plasma was spouted into them. The applied magnetic field was almost uniform. When the hydrogen was mixed with the discharging helium gas, the strong magnetic field was required to stabilize the discharge. The applied magnetic field B was set to 0.162 T, which was the maximum field strength in the apparatus.

Typical experimental conditions were the following: arc voltage 20–25 V (a little higher than for the pure helium plasma), arc current 120 A, pressure in the discharging region $P_{dc}=1.0\times10^4$–1.0×10^5 Pa, magnetic field $B=0.162$ T, gas flow rate 1.0×10^{-6}–4.0×10^{-6} kg/s, and the feeding ratio of the hydrogen molecule to the helium about 20–25 %. During generation of the plasma jet, the pressure in the wind tunnel P_{lc} was 3–20 Pa.

The account of the detection system is the following. The emission was observed along the direction perpendicular to the jet axis through the gaps of the coils. The light from the plasma was collected by a concave mirror of 30 mm diameter into an optical fiber terminal, fed to and analyzed by a monochromator-photomultiplier system (SS-50, systematized by JASCO corporation). The optical fiber assembly was a bundle of uv-grade fibers (ST-U200-DSY, manufactured by Mitsubishi Electric Wire Co.) and the diameter of the core was 200 μm. Its numerical aperture was 0.2. Before the light entered the monochromator, it was chopped at the rate of 270 Hz. The monochromator (fabricated by JASCO corporation, f 5.3) had a Czerny-Turner configuration, a focal length of 500 mm, and a linear reciprocal dispersion of 1.5 nm/mm. The widths of the entrance and exit slits were controllable and usually set 200 μm in the detection of emitted lines of Balmer series. The widths were chosen relatively wide in order to decrease of the photon-counting error and they could be closed to 2 μm if necessary. The heights of them were set 10 mm. The grooves of the grating of the monochromator was 1200/mm and the blaze wavelength of it was 500 nm. The output of the photomultiplier (R374, manufactured by Hamamatsu Photonics Corp. Ltd.) was fed to a preamplifier, whose output was led to a single-phase lock-in amplifier (5600 A, made by NF Electronic Instruments) and the electric signal was demodulated with the chopping signal. Finally, the output of the lock-in amplifier was converted into

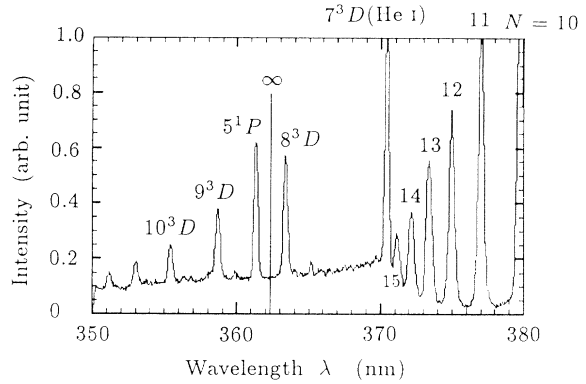

FIG. 1. Spectrum near the Balmer series limit. Marked with the angular momentum quantum number are the lines of He I. The spectrum sensitivity of the detection system is not calibrated for.

a digital signal and recorded by a 16-bit microcomputer (PC9801VM by NEC Corp.). The microcomputer also controlled the pulse motor which drove the grating and accomplished the acquisition of the data, conforming to the programmed sequence through a general-purpose interface-bus interface. The spectral sensitivity of the detection system had been calibrated by a standard halogen lamp (JPD100V500WCS, manufactured by Ushio Elec. Corp. and authorized by JEMIC) as an illuminance standard and a white standard reflectance plate (No. 6091 barium sulfate prepared by Eastman Kodak Co.) as a diffuse reflector, which acted as a luminance standard. The spectroscopic system was sensitive to the wavelength region of 250–870 nm. The diffracted lines of higher orders were cut off by optical filters.

III. RESULTS

The population densities of the excited hydrogen atoms with the principal quantum number $N \geq 3$ are obtained from the intensity integrated over the spectral peaks. The intensity of the Balmer lines was strong enough to neglect the background lines except for the transition $8 \rightarrow 2$, where the line of the transition $3\,^3P \rightarrow 2\,^3S$ of He I coincided with substantial intensity. It was difficult for us to measure the line intensity of the excited hydrogen atoms of $N = 8$. As mentioned later, the electron density of the plasma n_e is estimated at $\sim 10^{13}$ cm^{-3}, and the plasma is considered to be optically thin at least for the transitions to the level of $N = 2$. The temperature of the arc is considered as ~ 1 eV and the existence of He^{2+}

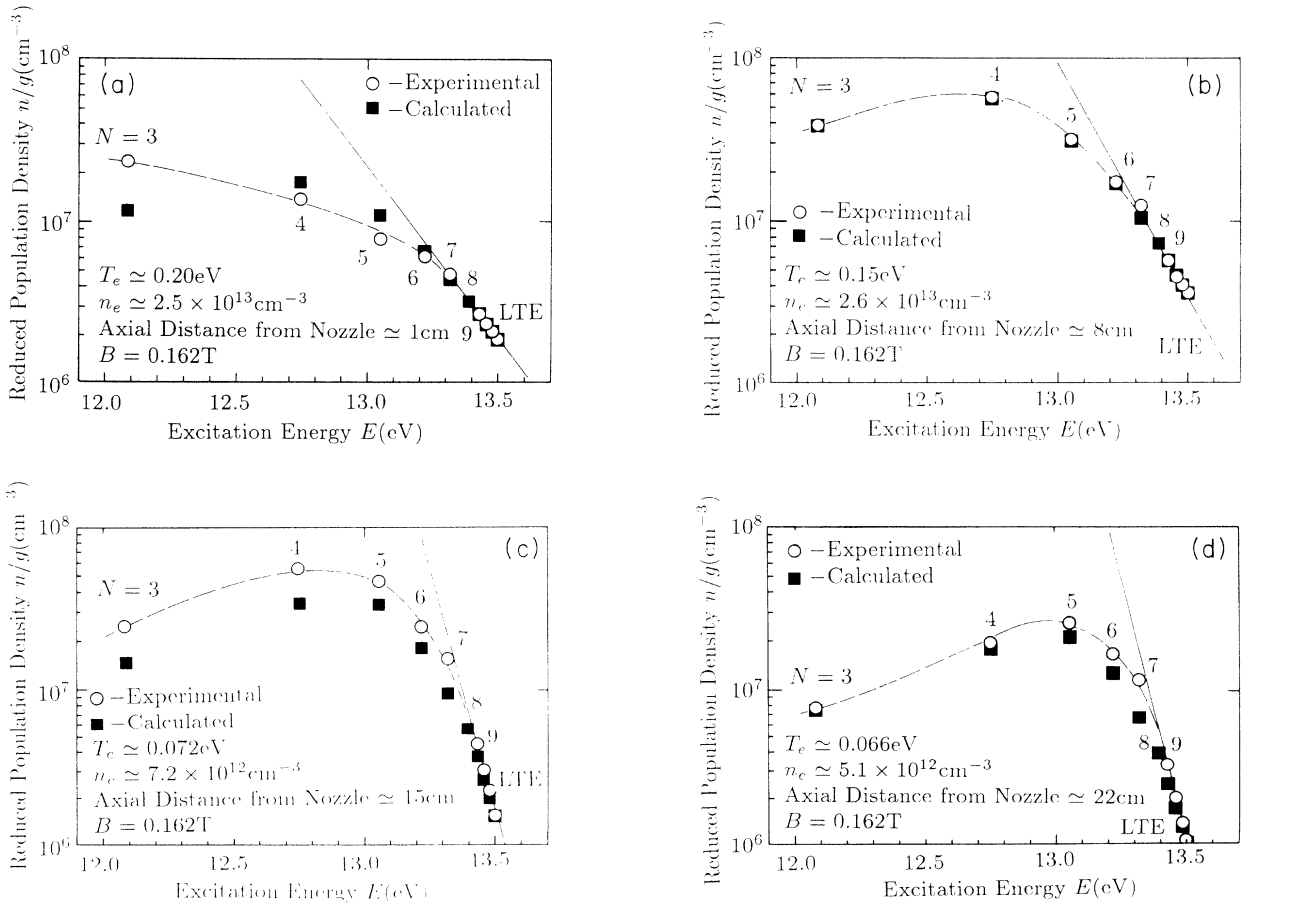

FIG. 2. Boltzmann plots of the populations of hydrogen atoms. The solid lines show the Saha-Boltzmann populations given by Eqs. (3) and (4). The pressure in the plasma expanding region $P_{lc} = 7.2$ Pa and the strength of the magnetic field $B = 0.162$ T. The pressure in the discharging region $P_{dc} = 1.0 \times 10^5$ Pa and the ratio of the hydrogen in it is about 0.2. The axial distance from the nozzle is 1, 8, 15, and 22 cm in (a), (b), (c), and (d), respectively. Calculated values are obtained through Eqs. (13)–(22) as functions of the observed electron temperature and density.

ions can be neglected. The line from the excited helium ion at 468.57 nm was not detected. Therefore the H_α line was observed precisely without the mixing of the 656.0-nm line of He II.

An example of the spectrum near the Balmer series limit is shown in Fig. 1. The lines from the large principal quantum number, particularly from $N \geq 13$, tend to merge with their neighboring lines and a continuumlike spectrum is obtained. Lines from the excited states of $N \geq 16$ cannot be separated if we intend to measure accurately without increasing the photon-counting error, and what is worse, the line of the $7\,^3D \rightarrow 2\,^3P$ transition in He I coincides at the wavelength from the excited hydrogen of $N = 16$. For the simple analysis of the experimental data, the population densities of the excited hydrogen atoms of $N \leq 12$ were determined experimentally. Figure 1 shows a strong continuum spectrum of free-bound transitions, and it means that the plasma is in a recombining phase neither in an ionizing phase nor in an equilibrium phase [23–27].

The reduced population densities n/g measured at some different positions are shown in Figs. 2(a)–2(d). ("Reduced" means that the population density n is divided by the statistical weight g.) The reduced population densities given there are the averaged value n/g along the line of sight from the condensing mirror directed to the plasma axis perpendicularly, that is,

$$\overline{n/g} = \left[\int_{\text{line of sight}} (n/g)dl\right] \Big/ \left[\int_{\text{line of sight}} dl\right] , \tag{1}$$

which is more essential in laser operation, and Abel inversion is not applied. The axial distance from the nozzle is (a) 1 cm, (b) 8 cm, (c) 15 cm, and (d) 22 cm. They correspond to the gap position of the coreless coils. Experimental errors are almost the same as the size of keys representing the reduced population densities of Fig. 2. The reproducibility of the experimental results lies within $\sim \pm 3\%$. We add there the electron temperature T_e and the electron density n_e, both of which were determined from the spectroscopic measurements and will be discussed later. The reduced population densities which are calculated as functions of the electron temperature and density, based on the collisional radiative model [23], are also added there. They will also be discussed in the latter part of this paper. One of the examples of the examined population densities of He I in the generated plasma is shown in Fig. 3, which was measured under the same conditions as in Fig. 2(b). Later we will show that the ion density of helium is about $\frac{1}{100}$ times that of hydrogen from Figs. 2(b) and 3.

To estimate the mean velocity of the plasma jet v, the Doppler shift of the H_α line (656.280 nm) was measured. A plane mirror was set downstream where the head-on view of the plasma was observed, and the reflected light was examined in the same way as the side-on view. The obtained spectral lines of H_α are shown in Fig. 4, where (a) is a side-on view and (b) is a head-on view. In the experiment, the slits were closed to 4 μm to improve the spectral resolution. It tells us that the blueshift of the

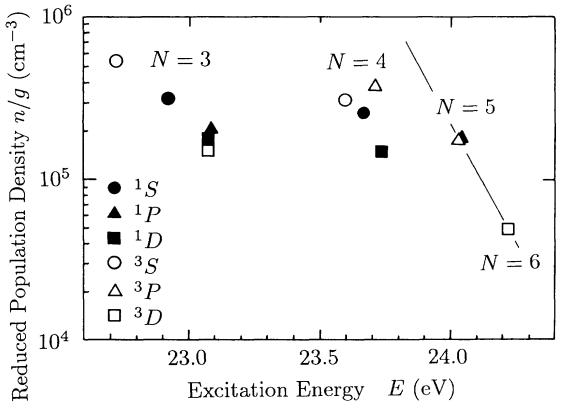

FIG. 3. Boltzmann plot of the populations of helium atoms. The solid line shows the Saha-Boltzmann populations given by Eqs. (3) and (4). Experimental conditions are the same as in Fig. 2(b).

line, about ~ 0.02 nm, was resolved. For the Doppler shift $\Delta\lambda$, we have

$$|\Delta\lambda|/\lambda = v/c , \tag{2}$$

where c is the speed of light. Therefore the mean velocity of the flow where the recombination radiant is dominant is evaluated at $\sim 9\times10^3 - 1\times10^4$ m/s.

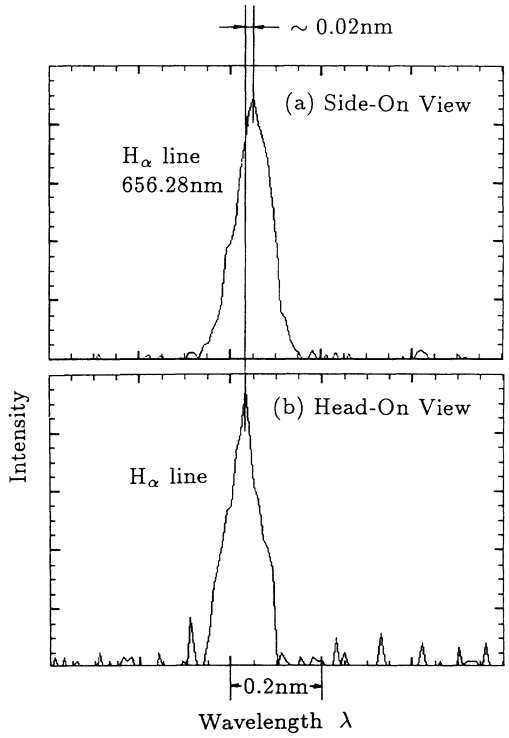

FIG. 4. The observed Doppler shift of H_α line. A side-on view gives the line (a), which does not shift, while a head-on view gives the line (b). The experimental conditions are the same as in Fig. 2. The slits of the monochromator are closed to 4 μm to improve the spectral resolution.

IV. DISCUSSION

A. Observed population inversion and potential for laser oscillation

Figure 2 clearly shows that the generated plasma was in a recombining phase. First, the high-lying levels of $N \geq 9$ tend to stay in local thermodynamic equilibrium (LTE). The Boltzmann plot there is on a straight line and the population densities of these high-lying levels are described by the Saha-Boltzmann equation

$$n(N)=n_e n_i(\mathrm{H}^+)Z(N)\ , \tag{3}$$

with

$$Z(N)=\frac{g(N)}{2g_i}\left[\frac{h^2}{2\pi mkT_e}\right]^{3/2}\exp\left[\frac{\chi(N)}{kT_e}\right]\ , \tag{4}$$

where n_i is an ion density, g_i is a statistical weight of the ion, h is the Planck constant, m is the electron mass, k is the Boltzmann constant, and $\chi(N)$ is the ionization potential of level N. $Z(N)$ is referred to as the Saha-Boltzmann coefficient [22,23].

Second, for the lower-lying levels, Eq. (3) gives too large population densities, which is the characteristic of the cold recombining plasma. And when the electron temperature T_e becomes low with an appropriate electron density n_e, the population inversion is obtained [18,26]. In the most upstream of the plasma jet, however, the population inversion was not obtained [Fig. 2(a)]. One of the reasons is that the electron temperature was not low enough there. Other reasons will be discussed later. Since the plasma is generated by an ordinary arc discharge under atmospheric pressure, it is considered that the plasma was in an equilibrium phase when it was generated, that is, at $z=0$ (z is the axial distance from the nozzle). As the plasma comes downstream, the population inversion appears gradually. The population inversion is observed between the level pair 4-3 at the position of the axial distance from the nozzle $z=8$ cm [Fig. 2(b)], between 4-3 and 5-3 at $z=15$ cm [Fig. 2(c)], and between 4-3, 5-3, 6-3, 7-3, and 5-4 at $z=22$ cm [Fig. 2(d)]. The variation of the population densities of these low-lying levels with the axial distance from the nozzle is shown in Fig. 5. It shows that the state of the plasma becomes far from the thermal equilibrium as the plasma comes downstream.

Another interpretation of Fig. 5 is that the figure shows the time history of the recombining plasma like an afterglow plasma. The plasma moves with the mean velocity $v \simeq 10^4$ m/s as described in Sec. III. If the plasma is assumed to move uniformly with the velocity, it takes 10 μs to move 10 cm. If the time origin ($t=0$) is set when the plasma passed through the nozzle, Fig. 2 shows the population densities of $t \simeq 1$ μs in (a), $t \simeq 8$ μs in (b), $t \simeq 15$ μs in (c), and $t \simeq 22$ μs in (d). The initial temperature of the plasma is considered ~ 1 eV from the probe analysis [19]. It means that the gas contact cooling is accomplished with the time scale of several microseconds, and it agrees with the simulation of gas contact cooling by Furukane, Sato, and Oda [15,28].

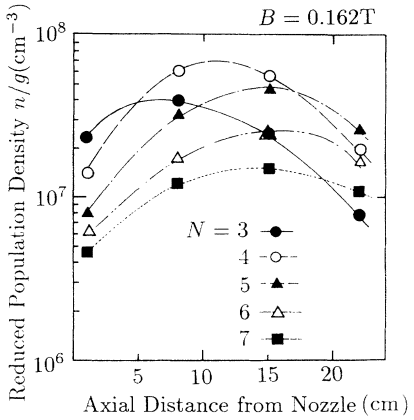

FIG. 5. Variation of the reduced population density n/g of levels $N=3-7$. Experimental conditions are the same as in Fig. 2.

When it is applied to the lasing medium, the important parameter is the reduced overpopulation density $\Delta[n/g(N_{\text{upper level}},N_{\text{lower level}})]$. Namely,

$$\Delta[n/g(N_1,N_2)]=[n(N_1)/g(N_1)]-[n(N_2)/g(N_2)]\ , \tag{5}$$

the subtraction is more essential than the quotient. The variations of the reduced overpopulation densities $\Delta(n/g)$ of the level pairs 4-3, 5-3, and 5-4 are shown in Fig. 6. In the present experiments, the maximum of the reduced overpopulation density is $\sim 3\times 10^7$ cm^{-3} for the level pair 4-3, $\sim 2\times 10^7$ cm^{-3} for 5-3, and 7×10^6 cm^{-3} for 5-4.

On the other hand, the threshold reduced overpopulation density for the laser oscillation $\Delta(n/g)_{\text{th}}$ is calculated as follows if the line has a Gaussian profile [17]:

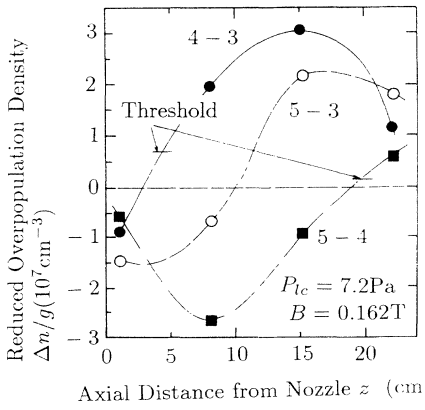

FIG. 6. Variation of the reduced overpopulation density $\Delta(n/g)$ between level pairs 4-3, 5-4, and 5-3. Experimental conditions are the same as in Fig. 2. The threshold value is calculated using Eq. (6).

$$\Delta[n/g(N_1,N_2)]_{\text{th}}=\frac{8\pi^{3/2}}{g(N_1)A(N_1,N_2)\lambda(N_1,N_2)^3}\times\left[\frac{2kT_{\text{H}}}{m_{\text{H}}}\right]^{1/2}\left[-\frac{\ln\sqrt{r_1r_2}}{L}\right], \tag{6}$$

where $A(N_1,N_2)$ is the transition probability $N_1\rightarrow N_2$, $\lambda(N_1,N_2)$ is the wavelength, m_{H} is the mass of the hydrogen atom, T_{H} is the temperature of the hydrogen atom (in K), r_1 and r_2 are the reflectivities of the cavity mirrors, and L is the distance of the mirrors and assumed to be the same as the length of the plasma region. We supposed the following values for the calculation: $T_{\text{H}}=700$ K (temperature of surrounding residual atom), $r_1=0.99$, $r_2=0.998$, and $L=5$ cm (the observed bright area). The threshold overpopulation densities calculated for the level pairs 4-3 and 5-4 are added in Fig. 6. It shows that the experimentally observed overpopulation densities of these level pairs were larger than the threshold values, whereas the observed values for any other level pairs, such as 5-3, did not surpass the threshold. If appropriate resonator mirrors are added to the apparatus, the laser oscillation of these lines is expected, which was not expected in pure helium plasma [20].

The obtained overpopulation densities of H I in our apparatus are larger than those reported in Refs. [7] and [9], where the magnetic confinement was not applied. It is concluded that the magnetic field is effective to enlarge the inversion. The electric power required for the discharge is about 3 kW in our apparatus, which is lower than those experiments. In the experiments of TPD-I [14,16], the hydrogen gas was not fed to the discharging region but to the plasma jet region. Although the inversion between the level pair 4-3 was larger in TPD-I than that in our apparatus, the efficiency to produce the hydrogen plasma in TPD-I was low because it was generated by contact with the helium plasma and the power about 13 kW was required. The advantages of our apparatus are summarized as follows: (1) It contains magnets to keep the electron density appropriate. (2) The expanding ratio of the jet is very large. The pressure of the discharging area is about 10^5 Pa and that of the expanding area is about 7 Pa. Therefore the neutral particles are expanded and cooled very rapidly. (3) The velocity of the jet is very large and considered to be supersonic due to the small diameter of the nozzle, which is considered to be choked with the viscous arc plasma. These are important to develop cw plasma jet lasers.

B. Macroscopic characteristics of the plasma

For the recombining plasma, the population densities of the sufficient high-lying levels are described by Saha-Boltzmann equation, namely, Eqs. (3) and (4). The electron temperature is determined from the gradient of the high-lying levels in Fig. 2. We used those with $N\geq 10$, and the reason will be discussed later. Then, since the detection system had been calibrated for absolutely, we determined the electron density from Fig. 2, provided that almost all the ions in the plasma are atomic hydrogen ions. Later it will be shown that the existence of the helium ions can be neglected.

In the present discussion, the existence of hydrogen molecular ions is also neglected. Since the plasma is in a recombining phase in the expanding region, the hydrogen molecules which are ionized there can be neglected. The formation of the molecular hydrogen ions through the reactions $H^+ + H^+ + e^- \rightarrow H_2^+$ or $H^+ + H \rightarrow H_2^+$ may be neglected because of their large relaxation times [28]. Even if there may be molecular hydrogen ions, they originate from the arc discharging region. Most of them are considered to be lost through the rapid dissociative recombination. The recombination coefficient of the molecular hydrogen ion was estimated at $\sim 3\times 10^{-8}$ cm^3/s, which was almost constant in the energy range $T_e \simeq 0.05$–2 eV [29]. On the other hand, the recombination rate coefficient of the atomic hydrogen ion is much smaller than that of the molecular ion and estimated at about 1×10^{-11}–1×10^{-10} cm^3/s [22]. When the plasma comes from the arc region to the expanding region, it is considered that the molecular ions recombine much faster (about 300–3000 times faster) than the atomic ions through the dissociative recombination. When 1 μs has passed since the plasma passed the nozzle, the existence of the molecular ions is almost negligible.

The extrapolated value of n/g to the ionization limit (13.6 eV for H I) $n/g(\infty)$ (in cm^{-3}) is derived from Eq. (3) as follows:

$$n_e n_i(\text{H}^+)=4.9\times 10^{15}[n/g(\infty)]T_e^{3/2}, \tag{7}$$

where T_e is in K and n_e and n_i are in cm^{-3}. From the condition of the neutrality,

$$n_e=n_i(\text{H}^+)+n_i(\text{He}^+). \tag{8}$$

Since the second term of the right-hand side of Eq. (8) is negligible as described later, n_e is obtained through Eqs. (7) and (8). The existence of He^{2+} ions is negligible as described beforehand. The obtained values of T_e and n_e are added in Fig. 2. The variation of the electron temperature and density is shown in Fig. 7. It shows the averaged value along the line of sight from the detector. Like Figs. 5 and 6, it shows the time histories of the electron temperature and density. The electron temperature becomes gradually lower as the plasma comes downstream. The important feature is that the cooling by the gas contact method requires several microseconds. This is also consistent with the simulation by Furukane, Sato, and Oda [15,28].

The density $n_i(\text{He}^+)$ is calculated from the results shown in Fig. 3 by extrapolating the value of n/g to the ionization limit of helium atom (24.5876 eV). The statistical weight of the helium ion is twice as large as the hydrogen ion, and Eq. (3) is applied to the helium plasma. And we find that the density of the helium ion is 5.1×10^{10} cm^{-3} in Fig. 3. It is about $\frac{1}{100}$ of the density of the hydrogen ion. Therefore it can be said that the density of the helium ions is much smaller than that of hydrogen ions in the plasma.

To confirm the assumption that the levels used in the

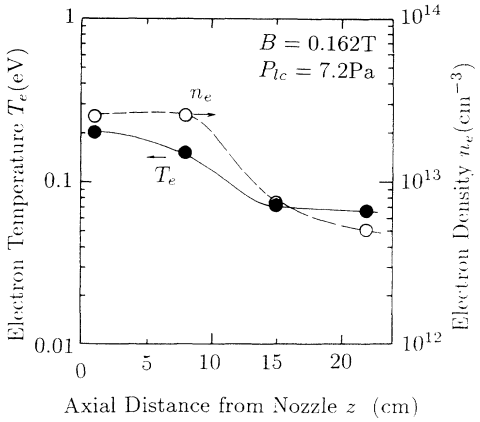

FIG. 7. Variations of the electron temperature T_e and n_e. Experimental conditions are the same as in Fig. 2.

calculation ($N \geq 10$) was in LTE, the validity criteria for LTE should be examined for the plasma in problem. Fujimoto and McWhirter showed that two criteria should be met for the justification of the LTE assumption, that is,

$$N \geq 118/T_e^{0.43} + 279/n_e^{0.15} \tag{9}$$

and

$$N \geq 282/T_e^{0.5} \tag{10}$$

for hydrogen plasmas in a recombining phase, where T_e is in K and n_e is in cm^{-3} [30]. These equations show that N should be equal to or larger than 7 in Fig. 2(a), 8 in Fig. 2(b), 10 in Figs. 2(c) and 2(d). Therefore our assumption met with the criteria. For levels lying lower than those determined by Eqs. (9) and (10), the experimental results show much smaller population densities than in the state of LTE. The appropriateness of the criteria Eqs. (9) and (10) is confirmed in the present experiments.

It was difficult for us to determine the gas temperature from the experiment. The applied magnetic field was rather weak and the plasma was assumed not to be magnetized. In the one-dimensional case, the plasma boundary moves with the velocity

$$v_m = 2v_0/(\gamma - 1) , \tag{11}$$

where v_0 is the sound velocity in atomic hydrogen and γ is the specific-heat ratio, if the plasma is assumed to be pure hydrogen atoms [31]. In the present experiment, the plasma is confined magnetically to the direction perpendicular to the flowing and approximated as one dimensional. Since v_m was estimated at about 9×10^3 m/s, Eq. (11) tells us that $v_0 \simeq 3\times10^3$ m/s. When the temperature of the atomic hydrogen T_H is given, v_0 can be calculated as follows:

$$v_0 = \sqrt{\gamma k T_H / m_H} . \tag{12}$$

Then it is considered that the temperature of the hydrogen atom is about 700 K. This gives a reasonable value. According to the simulation by Furukane, Sato, and Oda [15,28], the electron temperature cooled by the gas contact method becomes that of the contact gas after several microseconds have passed due to the collisional relaxation. In our experiments, the electron temperature becomes 0.066 eV =770 K at z =22 cm, where the duration of the contact is estimated at 22 μs. Therefore it is concluded that our experimental results agree with their simulation very well.

C. Comparison of the experimental results with the calculation based on the collisional radiative model

The electron temperature and density were obtained in Fig. 7. From these values, the population densities of the excited states of hydrogen atoms can be calculated by the collisional radiative model with the assumption that the plasma is optically thin [22]. In the present calculation, the method in Ref. [22] was used. For the rate coefficients of the excitation and the deexcitation by electronic collisions, the formula for electrons with the low temperature were used [32,33]. Later we will show how poor the Born approximation is to calculate population densities in the generated plasma. The deexcitation rate coefficient $F(N_1,N_2)$ (in cm^{3}s^{-1}) is formulated below [26]:

$$F(N_1,N_2) = 1.8\times10^{-6} T_e^{-0.17} N_2^{6.66} N_1^{-5} , \tag{13}$$

where T_e is in K. We use Eq. (13) for all the transitions. The excitation rate coefficient $C(N_1,N_2)$ is calculated from Eq. (13) using the detailed balance equation

$$C(N_1,N_2) = F(N_2,N_1) Z(N_2)/Z(N_1) . \tag{14}$$

As for the ionization rate coefficient from the ground state $S(1)$, the data by Bell *et al.* was used [34]. The classical scaling was employed for the ionization rate coefficients from the excited states [29]. That is,

$$S(N) = S(1) \left[\frac{R}{\chi(N)} \right]^2 , \tag{15}$$

where R is the Rydberg energy and equal to $\chi(1)$, and S is described as a function of $U = kT_e/\chi(N)$. From $S(N)$, the three-body recombination coefficient $\alpha(N)$ is calculated using the detailed balance equation. Namely,

$$\alpha(N) = S(N) Z(N) . \tag{16}$$

The radiative recombination coefficient $\beta(N)$ is calculated as follows [23]:

$$\beta(N) = \frac{2^4}{3\sqrt{3}} \frac{e^4}{m^2 c^3 \epsilon_0^2} \frac{1}{N^3} \left[\frac{R}{\pi k T_e} \right]^{3/2} \times \exp\left[\frac{\chi(N)}{kT_e} \right] \left[-\mathrm{Ei}\left[-\frac{\chi(N)}{kT_e} \right] \right] , \tag{17}$$

where e is the elementary electric charge, ϵ_0 is the permitivity of vacuum, and Ei is the exponential integral function, defined

$$-\mathrm{Ei}(-x) \equiv \int_x^\infty \frac{\exp(-t)}{t} dt . \tag{18}$$

The atomic transition probabilities $A(N_1,N_2)$ listed in

Ref. [21] are used. If the values for high-lying levels are not listed, $A(N_1,N_2)$ can be calculated by the well-known approximation of oscillator strength f for the excited states as follows [35]:

$$A(N_1,N_2)=\frac{2\pi e^2\nu^2}{mc^3\epsilon_0}\frac{g(N_2)}{g(N_1)}f_{N_2,N_1} \tag{19}$$

and

$$f_{N_2,N_1}=\frac{2^6}{3\sqrt{3}\pi}\frac{1}{g(N_2)}\frac{1}{N_1^3N_2^3}\frac{1}{(N_2^{-2}-N_1^{-2})^3}\ , \tag{20}$$

where ν is the frequency of the emitted lines. In the present calculation, the optical thicknesses are neglected. With these coefficients, the rate of variation of the population density $n(N_1)$ of level N_1 is described by the following equation [22]:

$$\frac{dn(N_1)}{dt}=\sum_{N=1}^{N_1-1}C(N,N_1)n(N)n_e+\left[\sum_{N=N_1+1}^{\infty}\{F(N,N_1)n_e+A(N,N_1)\}n(N)\right]+[\alpha(N_1)n_e+\beta(N_1)]n_en_i$$
$$-\left[\left\{\sum_{N=1}^{N_1-1}F(N_1,N)+\sum_{N=N_1+1}^{\infty}C(N_1,N)+S(N_1)\right\}n_e+\sum_{N=1}^{N_1-1}A(N_1,N)\right]n(N_1)\ . \tag{21}$$

Generally, the time derivative of the population densities of all the excited states ($N\geq 2$) may be set equal to 0 [22,23]. And in the present calculation, the population densities for all the levels above $N=35$ are supposed to be described by Eq. (3). From the practical viewpoint, the summations to infinity may be cut off at a sufficiently high-lying level N_∞, which is set at 40. Consequently, when the electron temperature and density are given, Eq. (21) is solved in the form

$$n(N)=Z(N)r_0(N)n_in_e+[Z(N)/Z(1)]r_1(N)n(1)\ , \tag{22}$$

where r_0 and r_1 are called the population coefficients and functions of n_e and T_e [23].

In an ionizing plasma like a positive column plasma, the second term of Eq. (22) is dominant. On the other hand, in a recombining plasma like an afterglow plasma, the first term is dominant [23–27]. Since the generated plasma in our experiments is evidently categorized into a recombining plasma and the electron temperature is sufficiently low, the second term of Eq. (22) can be neglected and the population densities of all the excited states are obtained even if the density of the ground state is left unknown. The results are added in Fig. 2.

Figure 2 shows that the results of the calculations agree well with the experimental results, particularly downstream [(b)–(d)]. Since the electron temperature of the plasma is very low, the rate coefficients are considered to contain considerable errors such as a factor of 2–3 [26]. But the agreement is very good, particularly in Figs. 2(b) and 2(d). Even in Fig. 2(c), the tendency of the variation of population densities with the principal quantum number is explained well by the calculation, and the deviation of the calculation from the experiment lies within a factor ~ 2. The experimental data are described satisfactorily by the collisional radiative model in which the plasma is optically thin in the downstream area, where the residual hydrogen atoms are considered to make diatomic molecule. Consequently, the absorption of the lines of Lyman series becomes less frequent and the plasma becomes optically thin, which is different from the helium plasma [20]. It resembles the phenomenon observed in an absolute calibration of a vacuum ultraviolet monochromator by the branching ratio method using hydrogen and helium lines [36].

From Eqs. (13)–(20), we can calculate the population rates and the depopulation frequencies of each elementary process. The results for the conditions in Fig. 2(b) and 2(d) are shown in Table I. These conditions were chosen because the agreement of the calculations with the experiments was very good and each of them represented the medium temperature condition [Fig. 2(b), $T_e=0.15$ eV] and the very low temperature condition [Fig. 2(d), $T_e=0.066$ eV]. In Table I, five population processes are treated separately, that is, radiative decay to the level N_1: $P_{ra}(N_1)$, collisional deexcitation $P_{cd}(N_1)$, collisional excitation $P_{ce}(N_1)$, three-body recombination $P_{3r}(N_1)$, and radiative recombination $P_{rr}(N_1)$, each of which is defined as follows:

$$P_{ra}(N_1)=\sum_{N=N_1+1}^{N_\infty}A(N,N_1)n(N)\ , \tag{23}$$

$$P_{cd}(N_1)=n_e\sum_{N=N_1+1}^{N_\infty}F(N,N_1)n(N)\ , \tag{24}$$

$$P_{ce}(N_1)=n_e\sum_{N=1}^{N_1-1}C(N,N_1)n(N)\ , \tag{25}$$

$$P_{3r}(N_1)=n_e^2n_i\alpha(N_1)\ , \tag{26}$$

$$P_{rr}(N_1)=n_en_i\beta(N_1)\ . \tag{27}$$

Likewise, four processes are treated separately in calculating depopulation frequencies, that is, radiative decay from the level N_1: $D_{ra}(N_1)$, collisional deexcitation $D_{de}(N_1)$, collisional excitation $D_{ce}(N_1)$, and ionization $D_{io}(N_1)$, each of which is defined as follows:

$$D_{ra}(N_1)=\sum_{N=1}^{N_1-1}A(N_1,N)\ , \tag{28}$$

$$D_{cd}(N_1)=n_e\sum_{N=1}^{N_1-1}F(N_1,N)\ , \tag{29}$$

$$D_{ce}(N_1)=n_e\sum_{N=N_1+1}^{N_\infty}C(N_1,N)\ , \tag{30}$$

$$D_{io}(N_1)=n_eS(N_1)\ . \tag{31}$$

We define total population rate P and total depopulation frequency D as follows:

$$P(N)=P_{ra}(N)+P_{cd}(N)+P_{ce}(N)+P_{3r}(N)+P_{rr}(N)\ , \tag{32}$$

$$D(N)=D_{ra}(N)+D_{cd}(N)+D_{ce}(N)+D_{io}(N)\ . \tag{33}$$

From Table I, it is found that the laser upper level populates mainly by the deexcitation processes from the highly excited states, which are populated dominantly through three-body recombinations. On the other hand, the laser lower levels depopulate more rapidly than the upper levels, mainly by radiative decay. [See level pairs 4-3 in Table I(a) and 5-4 and 4-3 in (b).] In the population processes, the collisional deexcitation process is most dominant for the laser upper levels [$N=4$ in Table I(a) and $N=4,5$ in (b)], while the radiative decay is the most dominant population process for the laser lower level [$N=3$ in (a) and (b)]. If the electron temperature is a little high, the collisional excitation process for high-lying levels becomes gradually significant [$N=5$ in (a)] and it is disadvantageous to form population inversion. As for the depopulation frequency, the total depopulation frequency for $N=5$ is about twice as large as that for $N=4$, and population inversion is not expected for the level pair in Table I(a). For level pairs 4-3 in (a) and any pairs in (b), the depopulation frequencies of the lower levels are larger than those of the upper levels.

It is seen that the tendency of the calculated population density is slightly different from the experiments in the most upstream area [Fig. 2(a)]. The calculation shows that the population inversion is expected between the level pair 4-3, but no inversion was observed in the experiments. It is supposed that the optical thickness to the ground state should be considered at least in the most upstream region, where hydrogen atoms with high density may exist without forming diatomic molecules. The expansion of hydrogen atoms is also insufficient in that region. Neutral hydrogen will expand very rapidly and form diatomic molecule downstream. In consequence, the optical thickness in the downstream can be neglected.

As for the rate coefficients, the electron temperature is very low in the present condition, therefore sufficient attention should be paid in calculating rate coefficients. Particularly, the rate coefficients of excitations and deexcitations by electron collisions [Eqs. (13) and (14)] are most critical in the present calculation. If we use the following excitation rate coefficients by Born approximation instead of Eq. (13), it makes the population densities of

TABLE I. Values for each component of the population rate and of the depopulation frequency under the conditions in Figs. 2(b) and 2(d). (a) shows them at middle T_e [correspondent to Fig. 2(b)] and (b) at very low T_e [Fig. 2(d)]. 1.2[9]=1.2×10⁹, etc.

(a) at $T_e=0.15$ eV and $n_e=2.6\times10^{13}$ cm^{-3} [Fig. 2(b), at middle T_e]

N	P/g (cm^{-3}s^{-1})	P_{ra}/g (cm^{-3}s^{-1})	P_{cd}/g (cm^{-3}s^{-1})	P_{ce}/g (cm^{-3}s^{-1})	P_{3r}/g (cm^{-3}s^{-1})	P_{rr}/g (cm^{-3}s^{-1})	n/g (cm^{-3})
3	4.2[15]	1.3[15]	3.0[15]	3.1[8]	9.6[12]	2.3[13]	4.0[7]
4	3.7[15]	1.9[14]	3.5[15]	9.4[12]	3.1[13]	9.1[12]	5.9[7]
5	4.1[15]	3.9[13]	3.6[15]	3.3[14]	7.7[13]	4.3[12]	3.3[7]

N	D (s^{-1})	D_{ra} (s^{-1})	D_{cd} (s^{-1})	D_{ce} (s^{-1})	D_{io} (s^{-1})
3	1.1[8]	1.0[8]	5.5[6]	4.6[5]	2.1[2]
4	6.3[7]	3.0[7]	2.1[7]	1.2[7]	5.5[4]
5	1.2[8]	1.2[7]	5.0[7]	6.2[7]	1.1[6]

(b) At $T_e=0.066$ eV and $n_e=5.1\times10^{12}$ cm^{-3} [Fig. 2(d), at very low T_e]

N	P/g (cm^{-3}s^{-1})	P_{ra}/g (cm^{-3}s^{-1})	P_{cd}/g (cm^{-3}s^{-1})	P_{ce}/g (cm^{-3}s^{-1})	P_{3r}/g (cm^{-3}s^{-1})	P_{rr}/g (cm^{-3}s^{-1})	n/g (cm^{-3})
3	7.3[14]	4.6[14]	2.6[14]	1.8[0]	1.6[11]	1.4[12]	7.2[6]
4	6.1[14]	1.2[14]	4.9[14]	1.4[9]	5.2[11]	5.7[11]	1.7[7]
5	5.2[14]	2.5[13]	4.9[14]	1.6[12]	1.3[12]	2.8[11]	2.1[7]

N	D (s^{-1})	D_{ra} (s^{-1})	D_{cd} (s^{-1})	D_{ce} (s^{-1})	D_{io} (s^{-1})
3	1.0[8]	1.0[8]	1.3[6]	3.5[2]	7.3[−5]
4	3.5[7]	3.0[7]	4.7[6]	1.6[5]	5.2[0]
5	2.5[7]	1.2[7]	1.1[7]	2.4[6]	1.3[3]

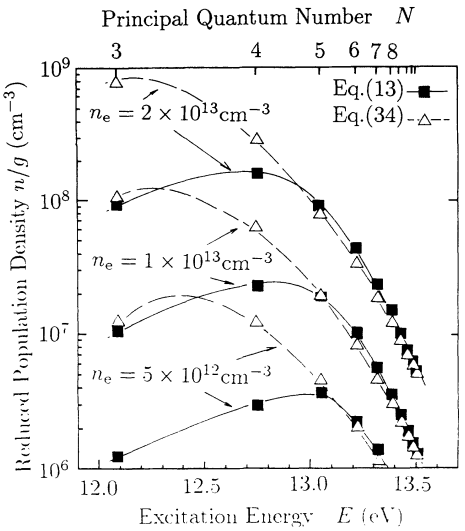

FIG. 8. Calculated reduced population densities n/g when the electron temperature T_e is 0.1 eV. The solid lines show them when Eqs. (13) and (14) are used for the excitation and deexcitation rate coefficients, which agree with the experiments very well. The dashed lines show them when Eq. (34) is used instead of Eq. (13).

the low-lying levels too large to explain the experimental results:

$$C(N_1,N_2)=G\frac{R}{\chi(N_1)-\chi(N_2)}f_{N_1,N_2} \times\exp\left[-\frac{\chi(N_1)-\chi(N_2)}{kT_e}\right], \quad (34)$$

with

$$G=4\pi a_0^2 R\left[\frac{1}{2\pi mkT_e}\right]^{1/2}, \quad (35)$$

where a_0 is the Bohr radius [23]. An example of the results is shown in Fig. 8 when the electron temperature is 0.1 eV. The calculation yields different results if we use Eq. (34) instead of Eq. (13). Equation (13) gives good results which agree with the experiments, while Eq. (34) gives poor results, especially for the population densities of the low-lying levels. It shows that the Born approximation is not valid in such low electron temperature as in our experiments. Equation (13) approximates the deexcitation rate coefficients with sufficient accuracy in the temperature range of the present experiments.

V. CONCLUSION

A stationary recombining hydrogen plasma was generated in the arc-heated magnetically trapped expanding plasma jet generator by mixing hydrogen gas into the discharging helium gas. The mixing ratio of hydrogen molecule to helium was about 20%. The plasma was generated very stably and the spectroscopic observation was accomplished with sufficient accuracy by a monochromator calibrated absolutely. Population densities of hydrogen atoms whose principal quantum number was 3-12 were observed. The plasma contained inverted populations in the plasma expanding region. Population inversions between level pairs 4-3, 5-3, 6-3, 7-3, and 5-4 were obtained in the downstream of the plasma jet. The inversion between level pairs 4-3 and 5-4 was so large that the cw laser oscillation would be expected with some appropriate resonator mirrors. The electric power required for the discharge was considerably low ($\sim$3 kW), which was enabled by the magnetic confinement, by the supersonic plasma flow, and by the effective cooling of the plasma due to the collisions with residual gas in the plasma expanding region. The electron temperature and density were determined from the population densities of high-lying levels, and the electron temperature was 0.06–0.2 eV and the density was 5×10^{12}–3×10^{13} cm^{-3}, both of which became gradually low when it came downstream. The mean velocity of the plasma jet was estimated from the Doppler shift of the jet, and it was about $\sim10^4$ m/s. The macroscopic characteristics were consistent with other authors' simulations of the gas contact cooling. The mixture ratio of the helium ion in the hydrogen ion was estimated at about $\frac{1}{100}$. The population densities of the excited states of hydrogen were calculated with a collisional radiative model as the functions of the observed electron temperature and density. In the calculation, the hydrogen plasma was assumed to be optically thin. The calculational results agreed very well with the experiments downstream.

ACKNOWLEDGMENTS

We thank Professor T. Fujimoto of Kyoto University for helpful discussions. We also thank Professor R. Shimada and Professor H. Yamasaki of our laboratory for their encouragement. The advice of Professor J. Heberlein of University of Minnesota is gratefully acknowledged. The collaborations by T. Goto, M. Ohta, T. Sone, H. Kinoshita, M. Komatsubara, and M. Hirayama are also acknowledged. Finally, we thank Mr. H. Miyabayashi for his technical support on this program. This work is partially supported by the Scientific Research Expenditure of the Japanese Ministry of Education.

[1] L. I. Gudzenko and L. A. Shelepin, Zh. Eksp. Teor. Fiz. **45**, 1445 (1963) [Sov. Phys. JETP **18**, 998 (1963)].
[2] S. Suckewer and H. Fishman, J. Appl. Phys. **51**, 1922 (1980).
[3] W. T. Silfvast and O. R. Wood II, J. Opt. Soc. Am. B **4**, 609 (1987).
[4] T. Hara, K. Ando, N. Kusakabe, H. Yashiro, and Y. Aoyagi, Jpn. J. Appl. Phys. **28**, L1010 (1989).
[5] E. M. Campbell, R. G. Jahn, W. F. von Jaskowsky, and K. E. Clark, J. Appl. Phys. **51**, 109 (1980).
[6] T. Hara, K. Kodera, M. Hamagaki, K. Matsunaga, M. Inutake, and T. Dote, Jpn. J. Appl. Phys. **19**, L606 (1980).
[7] V. M. Goldfarb, E. V. Ilyina, I. E. Kostygova, G. A. Lukyanov, and V. A. Silantyev, Opt. Spektrosk. **20**, 1085

(1966) [Opt. Spectrosc. (USSR) **20**, 602 (1966)].
[8] V. M. Goldfarb, E. V. Ilina, I. E. Kostygova, and G. A. Lukyanov, Opt. Spektrosk. **27**, 204 (1969) [Opt. Spectrosc. (USSR) **27**, 108 (1969)].
[9] P. Hoffmann and W. L. Bohn, Z. Naturforsch. A **27**, 878 (1972).
[10] S. W. Bowen and C. Park, AIAA J. **10**, 522 (1972).
[11] K. Sato, J. Phys. Soc. Jpn. **43**, 1027 (1977).
[12] K. Sato, M. Shiho, M. Hosokawa, H. Sugawara, T. Oda, and T. Sasaki, Phys. Rev. Lett. **39**, 1074 (1977).
[13] G. M. Zhinzhikov, G. A. Luk'yanov, V. V. Nazarov, and N. O. Pavlova, Zh. Tekh. Fiz. **48**, 949 (1978) [Sov. Phys. Tech. Phys. **23**, 554 (1978)].
[14] M. Otsuka, R. Ikee, and K. Ishii, J. Quant. Spectrosc. Radiat. Transfer **15**, 995 (1975).
[15] U. Furukane, K. Sato, and T. Oda, J. Phys. D **22**, 390 (1989).
[16] K. Sato, Rev. Laser Eng. **19**, 508 (1991) (in Japanese).
[17] T. Oda and U. Furukane, J. Quant. Spectrosc. Radiat. Transfer **29**, 553 (1983).
[18] U. Furukane and T. Oda, J. Quant. Spectrosc. Radiat. Transfer **33**, 645 (1985).
[19] H. Akatsuka and M. Suzuki, Rev. Sci. Instrum. **64**, 1734 (1993).
[20] H. Akatsuka and M. Suzuki, J. Quant. Spectrosc. Radiat. Transfer (to be published).
[21] W. L. Wiese, M. W. Smith, and B. M. Glennon, *Atomic Transition Probabilities, Vol. 1. Hydrogen Through Neon,* Natl. Bur. Stand. Ref. Data Ser., Natl. Bur. Stand. (U.S.) Circ. No. 4 (U.S. GPO, Washington, DC, 1966).
[22] T. Fujimoto, I. Sugiyama, and K. Fukuda, Mem. Fac. Eng. Kyoto Univ. **34**, 249 (1972).
[23] T. Fujimoto, J. Phys. Soc. Jpn. **47**, 265 (1979).
[24] T. Fujimoto, J. Phys. Soc. Jpn. **47**, 273 (1979).
[25] T. Fujimoto, J. Phys. Soc. Jpn. **49**, 1561 (1980).
[26] T. Fujimoto, J. Phys. Soc. Jpn. **49**, 1569 (1980).
[27] T. Fujimoto, J. Phys. Soc. Jpn. **54**, 2905 (1985).
[28] U. Furukane, K. Sato, and T. Oda, Jpn. J. Appl. Phys. **29**, 1814 (1990).
[29] H. W. Drawin, Association Euratom–CEA Report No. EUR-CEA-FC-383, 1967 (unpublished).
[30] T. Fujimoto and R. W. P. McWhirter, Phys. Rev. A **42**, 6588 (1990).
[31] L. I. Gudzenko, S. S. Filippov, and L. A. Shelepin, Zh. Eksp. Teor. Fiz. **51**, 1115 (1966) [Sov. Phys. JETP **24**, 745 (1967)].
[32] P. Manschbach and J. Keck, Phys. Rev. **181**, 275 (1969).
[33] F. Devos, J. Boulmer, and J.-F. Delpech, J. Phys. (Paris) **40**, 215 (1979).
[34] K. L. Bell, H. B. Gilbody, J. G. Hughes, A. E. Kingston, and F. J. Smith, J. Phys. Chem. Ref. Data **12**, 891 (1983).
[35] A. Unsöld, *Physik der Sternatmosphären,* 2nd ed. (Springer-Verlag, Berlin, 1955).
[36] S. Kasai, A. Funahashi, S. Konoshima, M. Nagami, T. Sugie, and K. Mori, Jpn. J. Appl. Phys. **17**, 1625 (1978).